Electronic Supplementary Material (ESI) for Chemical Science.

Sonophore-enhanced nanoemulsions for optoacoustic imaging of cancer

Sheryl Roberts[1, τ], Chrysafis Andreou[1, τ], Crystal Choi[1], Patrick Donabedian[1], Madhumitha Jayaraman[1], Edwin C. Pratt[2], Jun Tang[3], Carlos Pérez-Medina[4], Michael J. de la Cruz[5], Willem J. M. Mulder[4, 6], Jan Grimm[1,2,7,8], Moritz Kircher[1,2,7], Thomas Reiner*[,1,7]

[1] Department of Radiology, Memorial Sloan Kettering Cancer Center, New York, NY, 10065, USA

[2] Department of Molecular Pharmacology, Memorial Sloan Kettering Cancer Center, New York, NY, 10054, USA

[3] Cancer Research Institute (CRI), 29 Broadway, New York, NY, 10006, USA

[4] Translational and Molecular Imaging Institute, Department of Radiology, Mount Sinai School of Medicine, New York, NY, 10029, USA

[5] Structural Biology Program, Sloan Kettering Institute, Memorial Sloan Kettering Cancer Center, New York, New York, 10065, USA

[6] Department of Medical Biochemistry, Academic Medical Center, Amsterdam, The Netherlands

[7] Department of Radiology, Weill Cornell Medical College, New York, NY 10065, USA

[8] Pharmacology Program, Weill Cornell Medical College, New York, NY, 10065, USA

[τ] These authors contributed equally to this work

* Corresponding author

Supplementary information

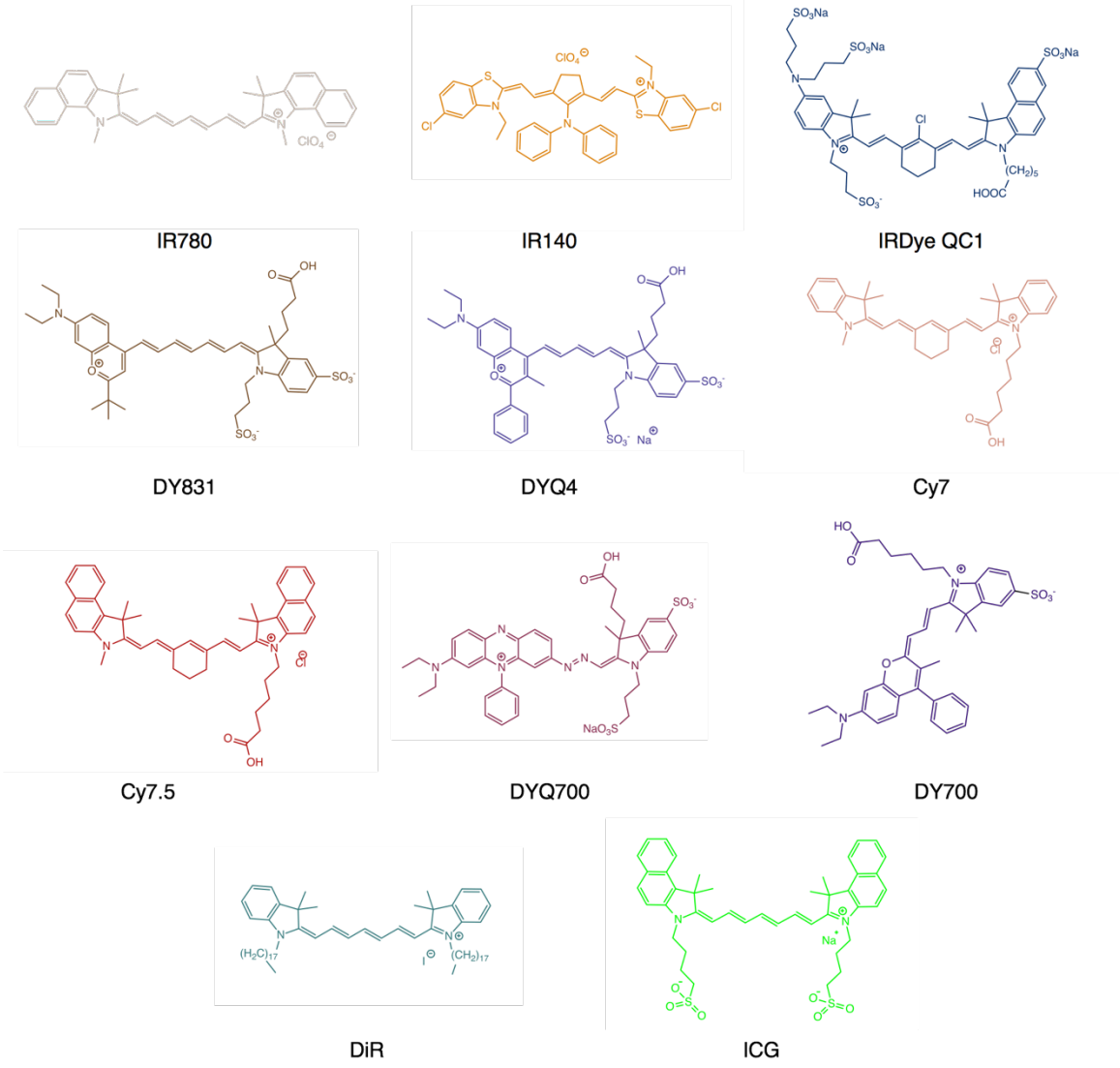

Figure S1: **The chemical library and structures of sonophores. Low fluorescent and** near-infrared dyes (IR780 perchlorate, IR140, Atto740 (structure not available), DY831, Cy7, Cy7.5, DY700, DiR and ICG) and dark quenchers (IRDye QC1, DYQ4 and DYQ700) were selected for screening.

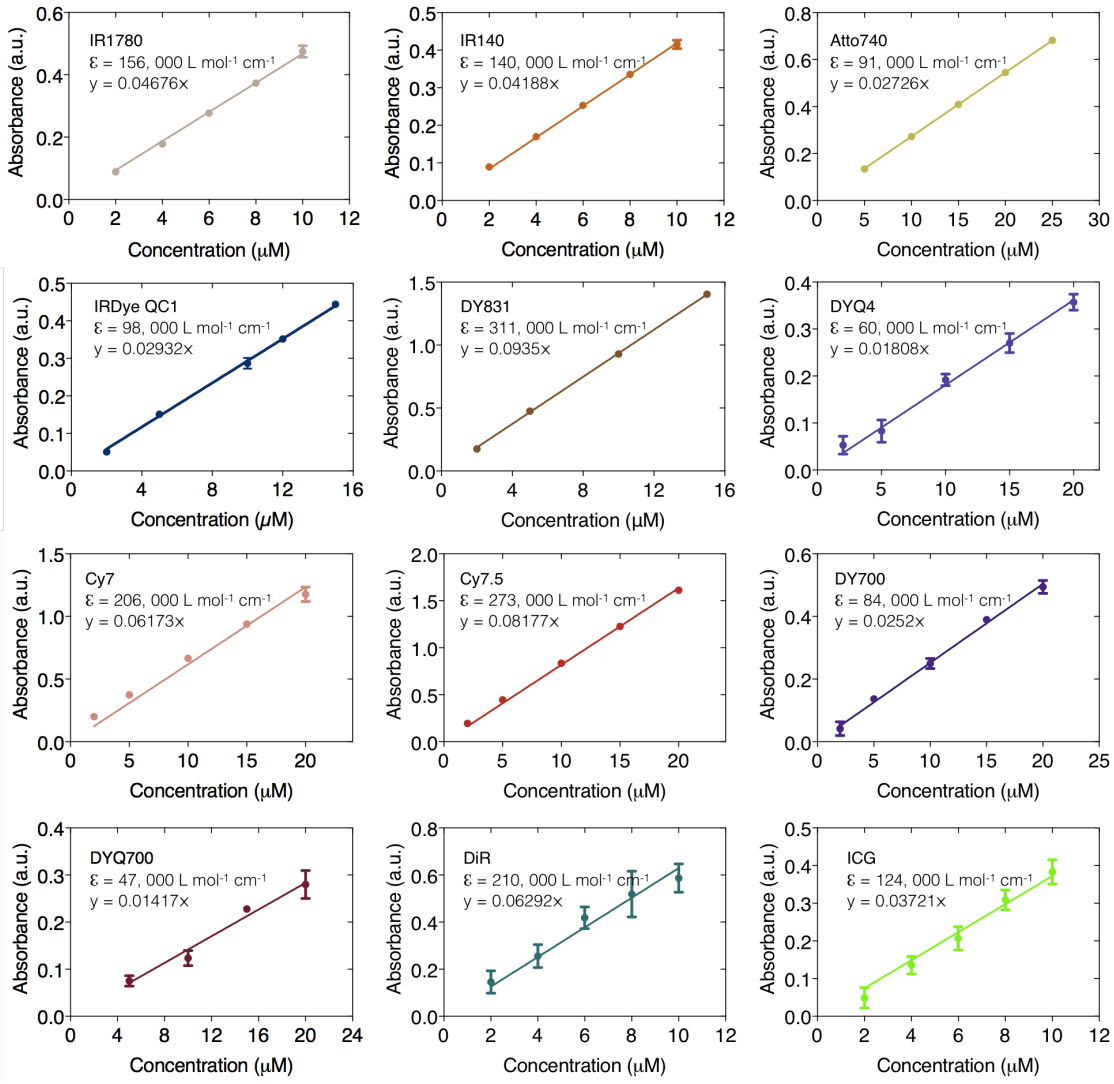

Figure S2: **Calibration curves from UV/Vis absorbance of near-infrared sonophores in DMSO.** The absorbance was measured at varying concentrations (μM) of near-infrared sonophores as indicated on the graph. The extinction coefficient was determined using the slope calculated for each dye.

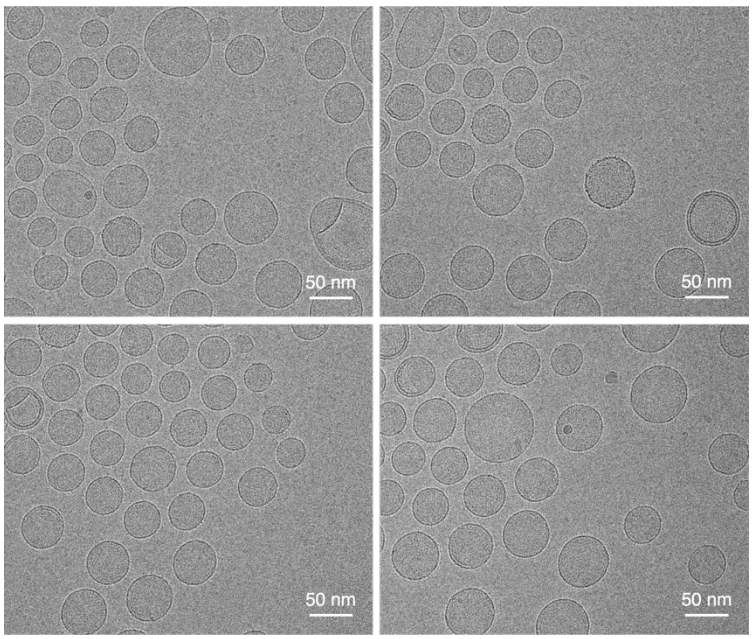

Figure S3: **Structural determination of near-infrared IRDye QC1 nanoemulsion with cryogenic transmission electron microscopy (cryo-TEM)**. Two-dimensional projection images of vitrified nanoemulsion. Images were taken at a nominal magnification of 18000× with super-resolution pixel size of 0.571 Å/px.

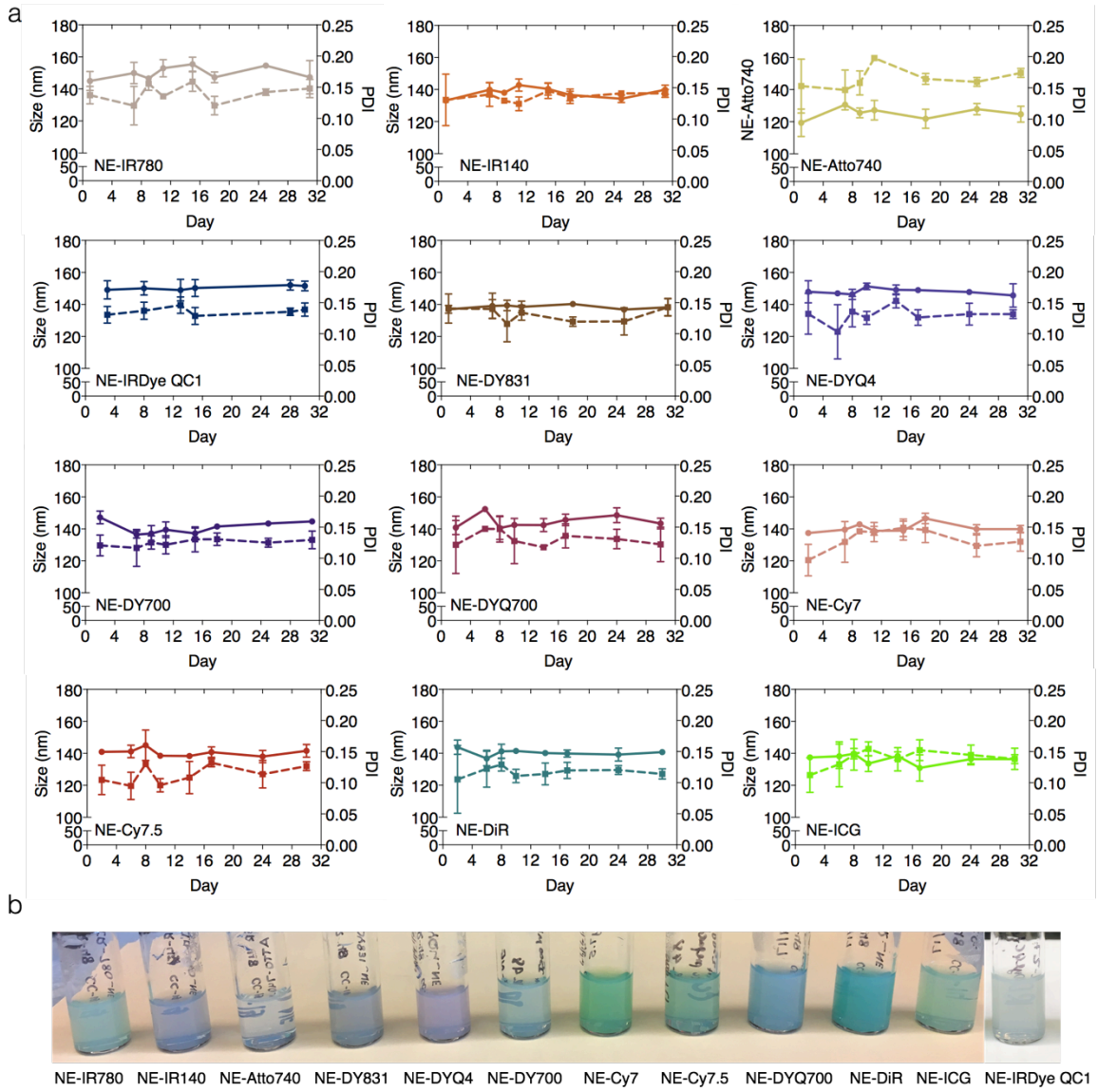

Figure S4: **Physical characterization of the near-infrared nanoemulsions over time.** Using dynamic light scattering (DLS), the size (*solid line*) and polydispersity index (pdi, *dotted line*) of the near-infrared nanoemulsions were measured over 30-32 days. The samples were stored in the dark at 4 ^{o}C in between measurements. The results show little change or no change (<5%) in size and pdi of the nanoemulsions, indicating that they are stable in formulation. (b) Images of near infrared nanoemulsions of oil-in-water system in the form of droplets with diameter in the nanometer range.

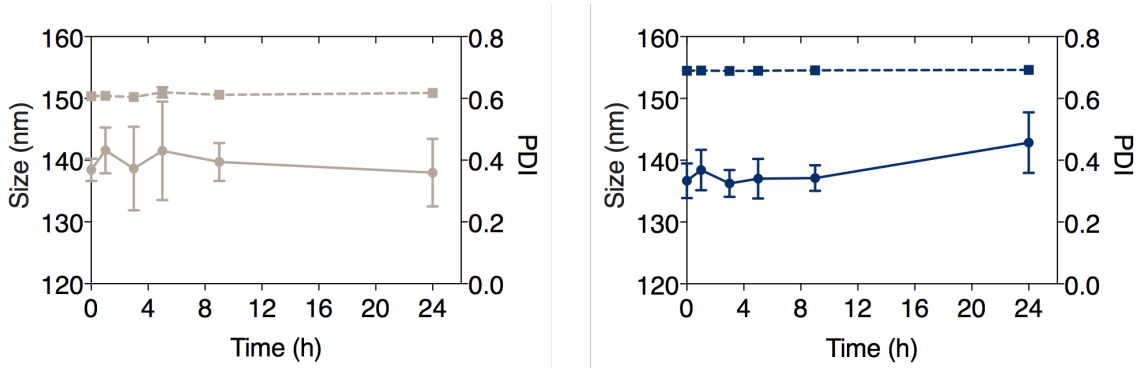

Figure S5: **Physical characterization of near-infrared nanoemulsions in albumin bovine serum (BSA) over time.** Using dynamic light scattering (DLS), the size (*solid line*) and polydispersity index (pdi, *dotted line*) of the near-infrared nanoemulsion NE-IR780 and NE-IRDye QC1 were measured over 24 h. The samples were stored in the dark at 4 ^{o}C in between measurements. The results show little change (<5%) in size of nanoemulsions, indicating that they are stable in formulation. In BSA, the size distribution appears more polydisperse possibly due to the formation of a protein corona on the nanoemulsions. The pdi of the nanoemulsions increased from approximately 0.15 to 0.60 as soon as it is in serum, but it does not change over time.

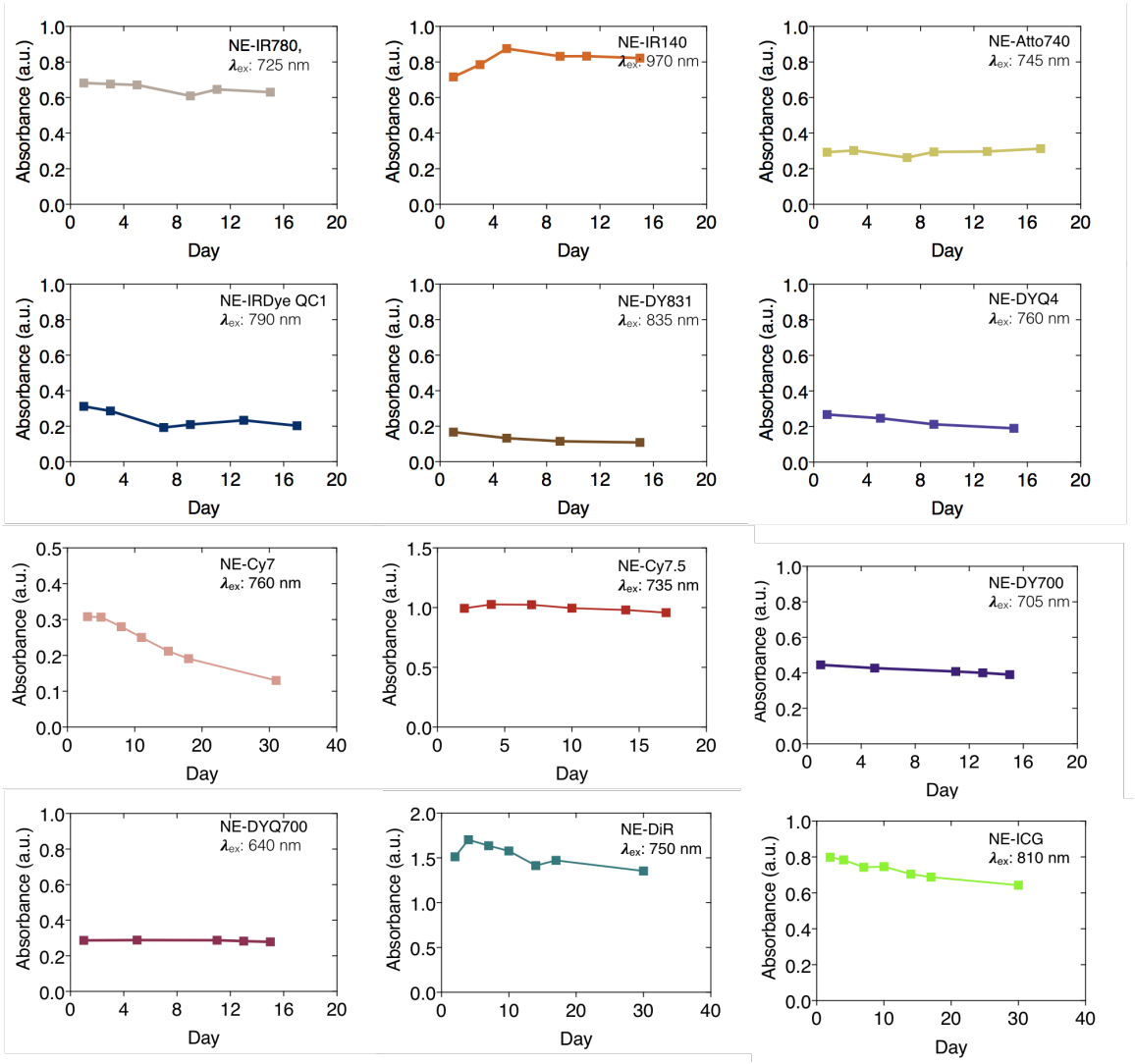

Figure S6: **Photostability study of the near-infrared nanoemulsions in phosphate buffer saline (PBS) over time, namely NE-IR780, NE-IR140, NE-Atto740, NE-IRDye QC1, NE-DY831, NE-DYQ4, NE-DY700 and NE-DYQ700.** The UV/Vis absorbance of the nanoemulsions was measured (350–1000 nm, 5 nm step wavelength resolution) and monitored over 15 days. The data were background corrected to PBS. The plots of the absorbance maxima *vs.* time (days) indicate the photostability of the near-infrared nanoemulsions in PBS.

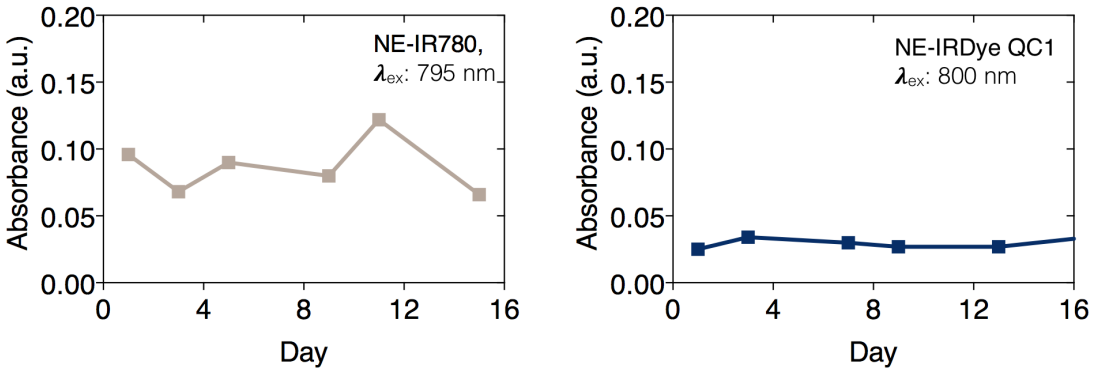

Figure S7: **Photostability study of near-infrared nanoemulsions NE-IR780 and NE-IRDyeQC1 in bovine serum albumin (BSA) over time.** The UV/Vis absorbance of the near-infrared nanoemulsions was measured (350–1000 nm, 5 nm step wavelength resolution) and monitored over 15–17 days. The data were background corrected to BSA. The plots of the absorbance maxima *vs.* time (days) indicate the photostability of the near-infrared nanoemulsions in BSA.

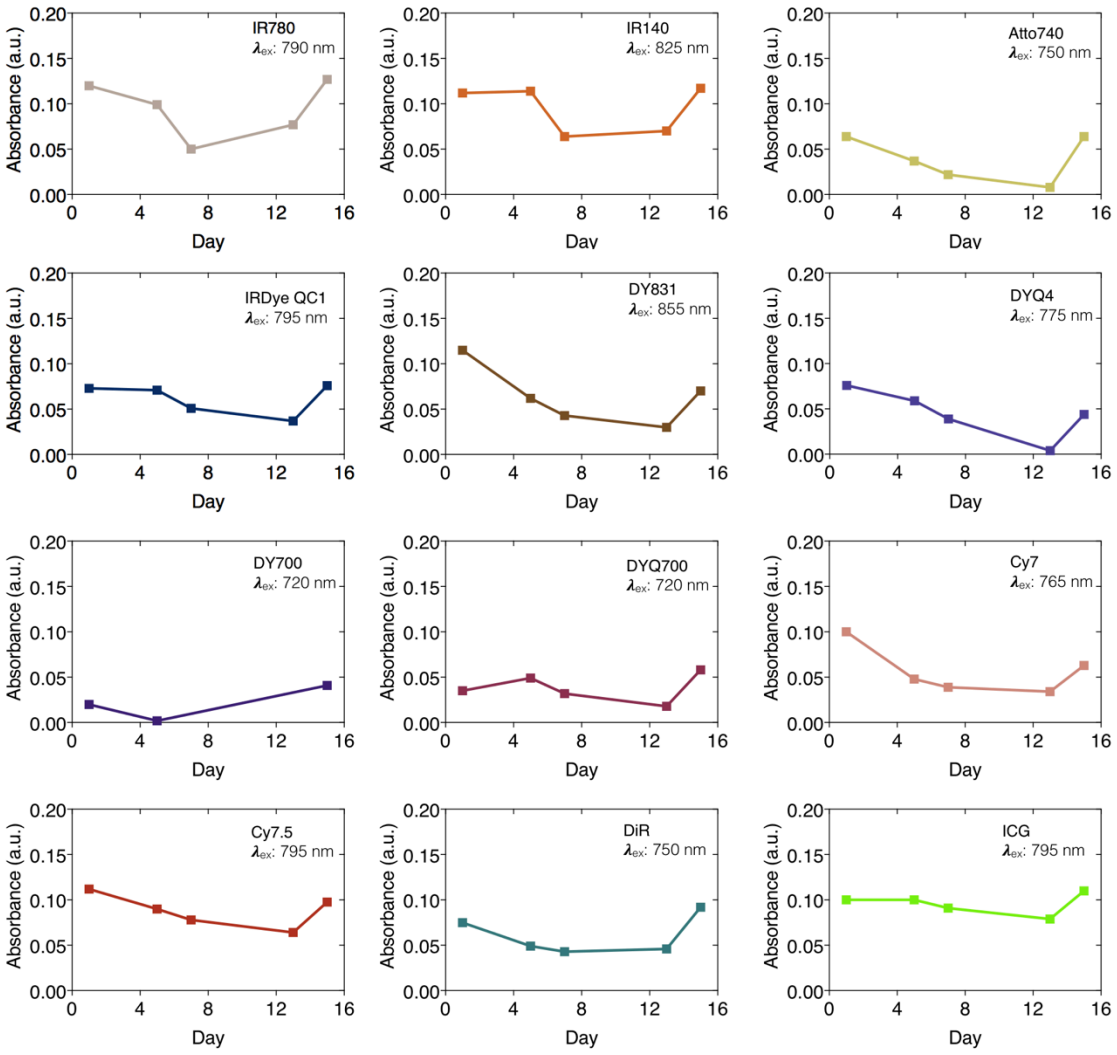

Figure S8: **Photostability study of near-infrared dyes IR780, IR140, Atto740, IRDye QC1, DY831, DYQ4, DY700, DYQ700, Cy7, Cy7.5, DiR and ICG in phosphate buffer saline over time.** The UV/Vis absorbance of the near-infrared dyes were measured (350–1000 nm, 5 nm step wavelength resolution) and monitored over 15–17 days. The data were background corrected to PBS. The plot of the absorbance maxima *vs.* time (days) indicates the photostability of the near-infrared dyes in PBS.

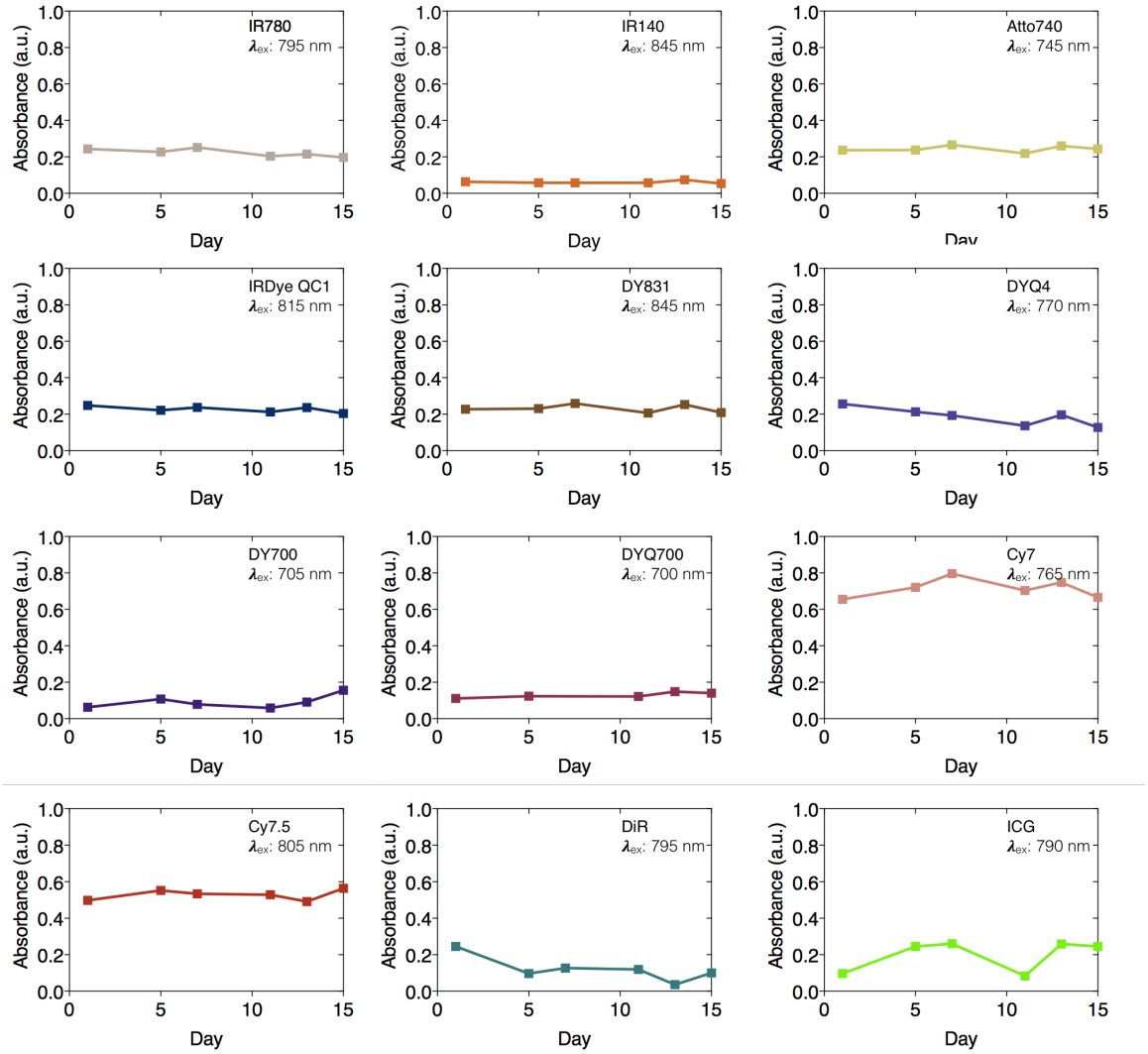

Figure S9: **Photostability study of the near-infrared dyes in bovine serum albumin (BSA) over time, namely IR780, IR140, Atto740, IRDye QC1, DY831, DYQ4, DY700, DYQ700, Cy7, Cy7.5, DiR and ICG.** The UV/Vis absorbance of the near-infrared dyes were measured (350- 1000 nm, 5 nm step wavelength resolution) and monitored over 15-17 days. The data was background corrected to BSA. The plot of the absorbance maxima *vs.* time (days) indicates the photostability of the near-infrared dyes in BSA.

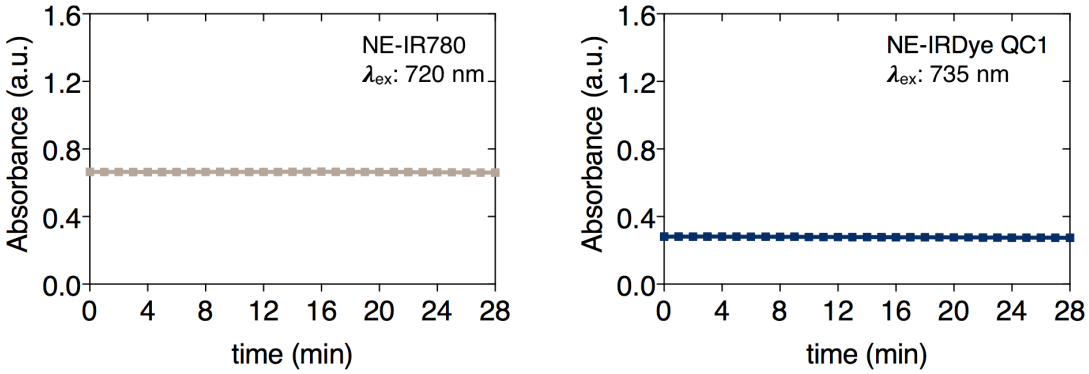

Figure S10: **Photostability study of near-infrared nanoemulsions in phosphate buffer saline (PBS) over time, namely NE-IR780 and NE-IRDye QC1.** The near-infrared nanoemulsions were irradiated with continuous light for 28 mins, excited at their maxima absorbance indicated on the graph. The UV/Vis absorbance at the maxima absorbance of the near-infrared nanoemulsions were plotted over 28 mins, indicating lack of photobleaching upon laser illumination at maximum absorbance.

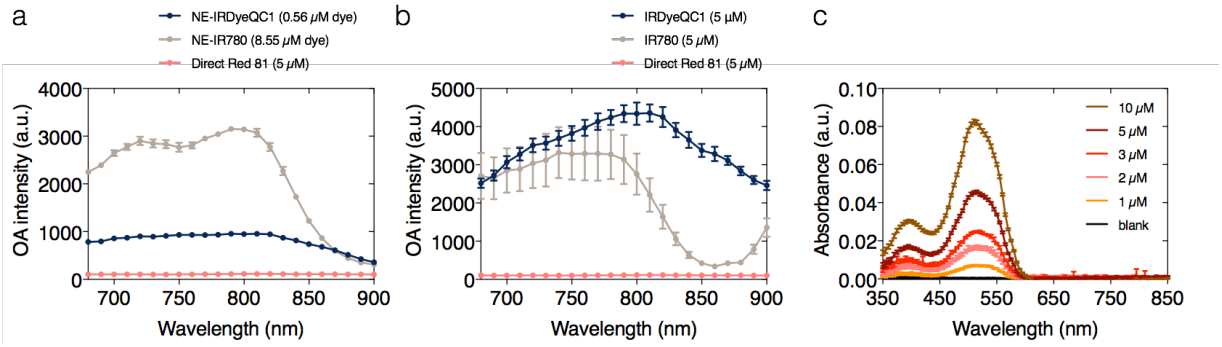

Figure S11: **Soft tissue mimicking phantoms have little or no effect on spectral coloring due to light fluence** (a) OA spectra from 680–900 nm (10 nm resolution) of NE-IRDyeQC1 (0.56 μM), NE-IR780 (8.55 μM) compared to Direct Red 81 (5 μM), at the concentrations used in soft tissue mimicking phantoms. (b) OA spectra (680–900 nm,10 nm resolution) comparison between IRDyeQC1 (5 μM), IR780 (5 μM) and Direct Red 81 (5 μM). (c) The UV/Vis absorption spectra of Direct Red 81 at 1 μM, 2 μM, 3 μM, 5 μM and 10 μM concentrations in phosphate saline buffer (PBS) showing a 501 nm maximum absorbance in the visible region and no absorbance contribution in the near-infrared region.

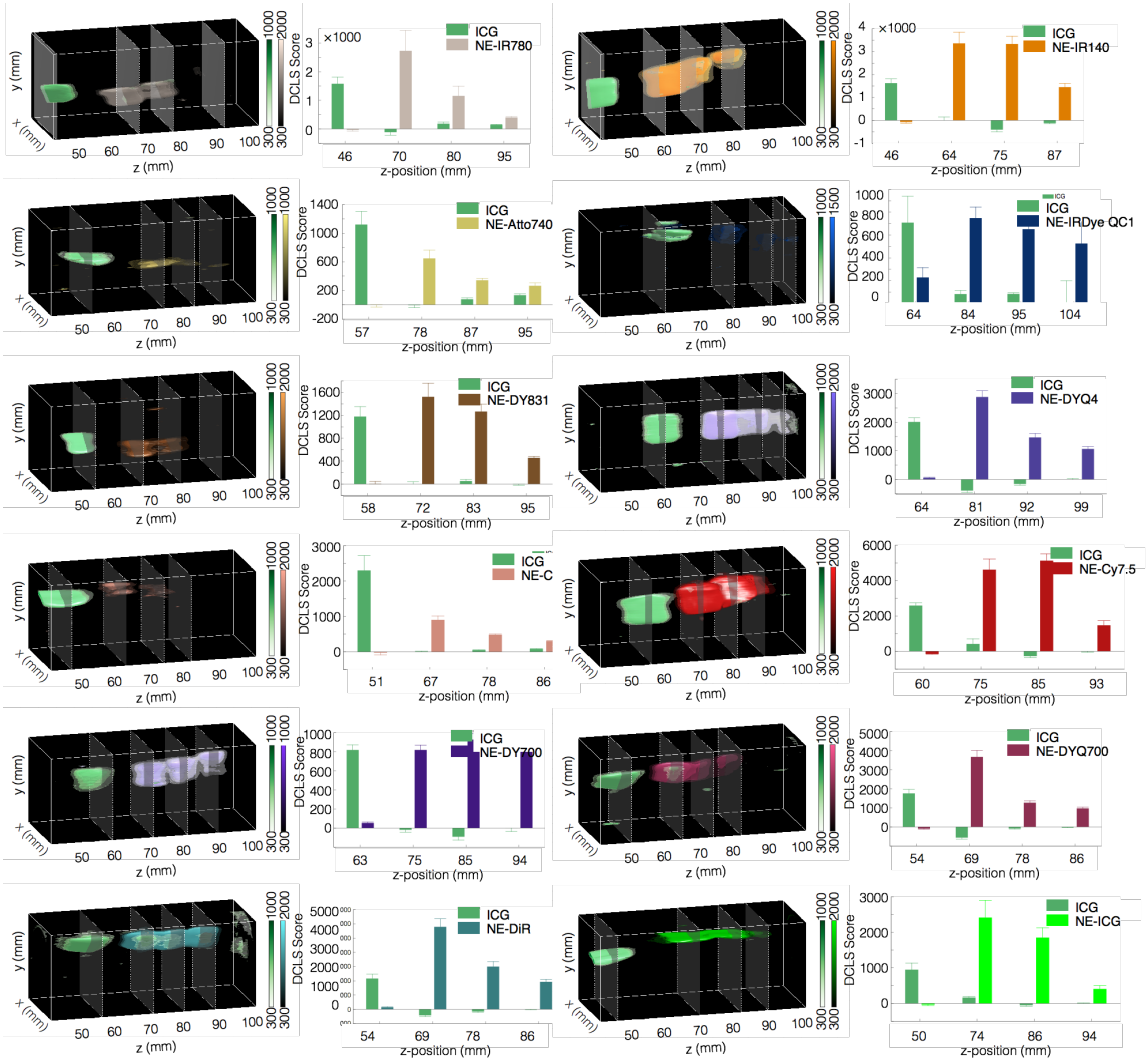

Figure S12: **MSOT imaging of near-infrared nanoemulsions in soft tissue mimicking phantoms.** The twelve nanoemulsion sonophores were imaged using MSOT. Optoacoustic reference spectra (Supporting Fig. S13, and Fig. 2d) were used as references for spectral unmixing using DCLS. The 3D reconstruction (*left column*) and the quantitation of ROIs (*right column*) show the specific detection and signal response of each nanoemulsion at the three serial dilutions (high, medium and low).

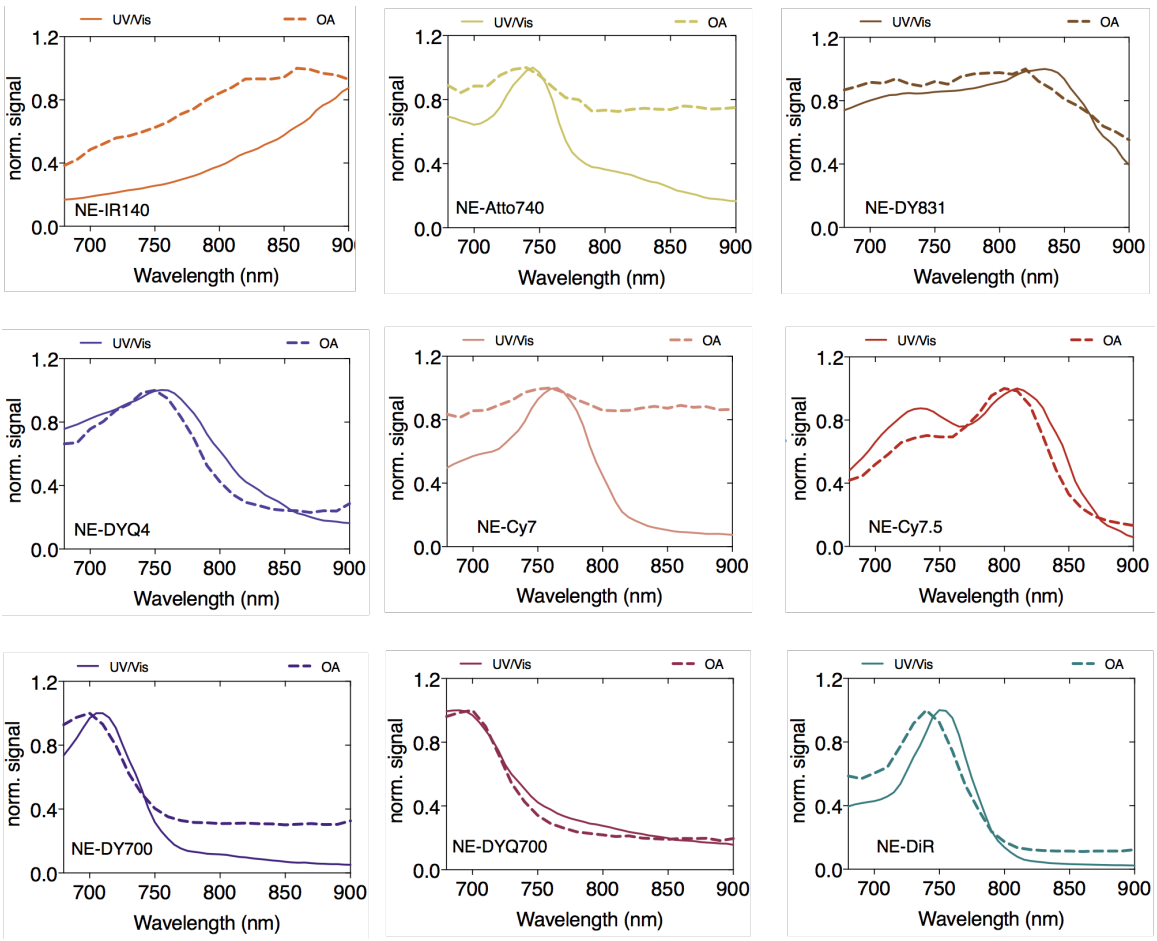

Figure S13: **Absorbance and optoacoustic spectra of near-infrared nanoemulsions, encapsulating the following sonophore: IR140, Atto74, DY831, DYQ4, Cy7 COOH, Cy7.5 COOH, DY700 COOH, DYQ700 COOH and DiR,.** UV/Vis absorbance (solid lines) and phantom MSOT measurements (dashed lines) of near-infrared nano emulsions at their highest concentrations**.** Measurements were carried out from 690–900 nm based on the corresponding optoacoustic imaging capabilities of the MSOT. The data were normalized to the absorbance and optoacoustic maximum of individual sonophores. See Supporting Table 1.

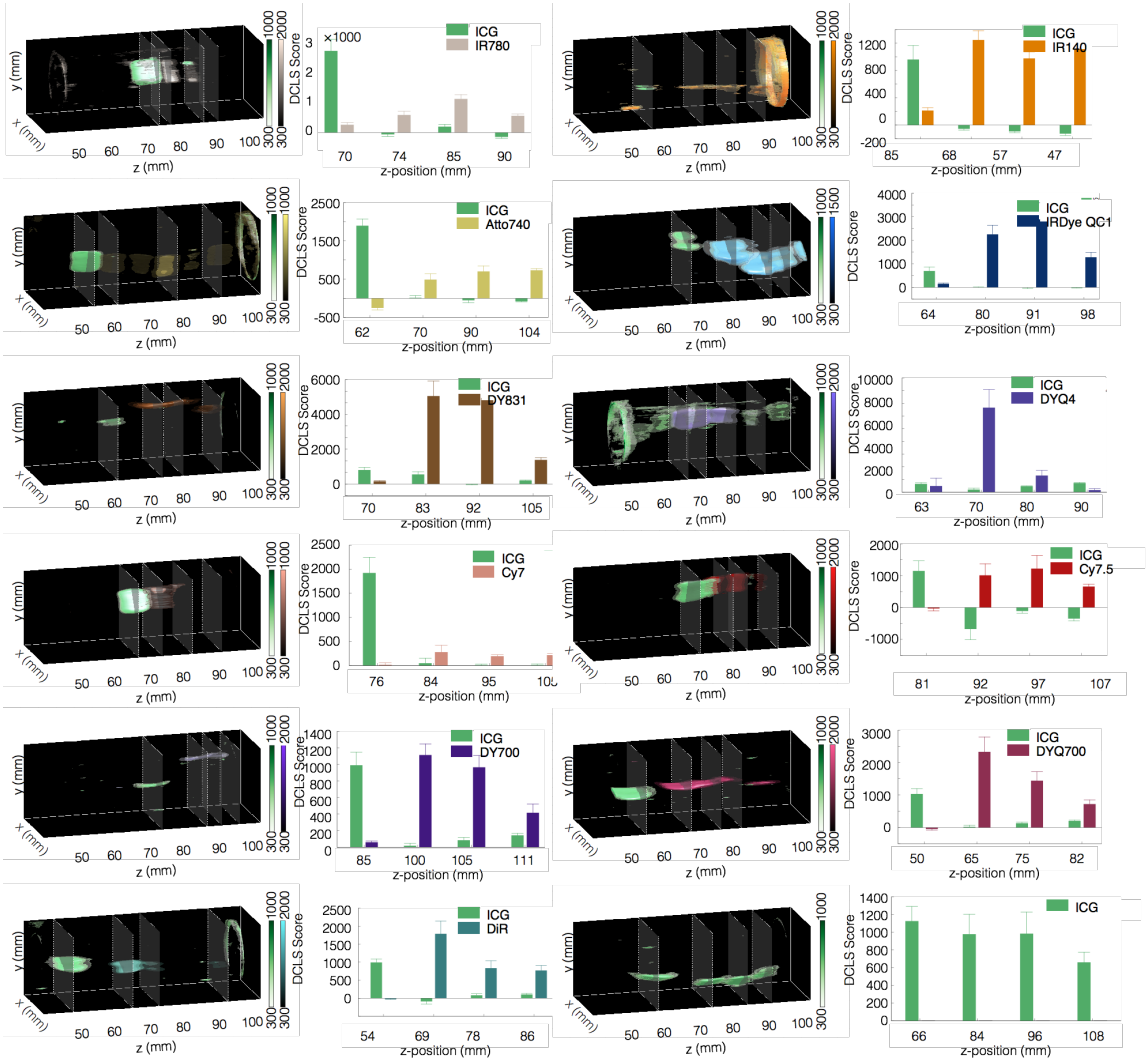

Figure S14**: MSOT imaging of the small molecule dyes in tissue mimicking phantoms.** Twelve small molecule sonophores were imaged using MSOT. Optoacoustic reference spectra (Supporting Fig. S15) were used as references for spectral unmixing using DCLS. The 3D reconstruction (*left column*) and the quantitation of ROIs (*right column*) show the specific detection and signal response of each sonophore at the three serial dilutions (high, medium and low).

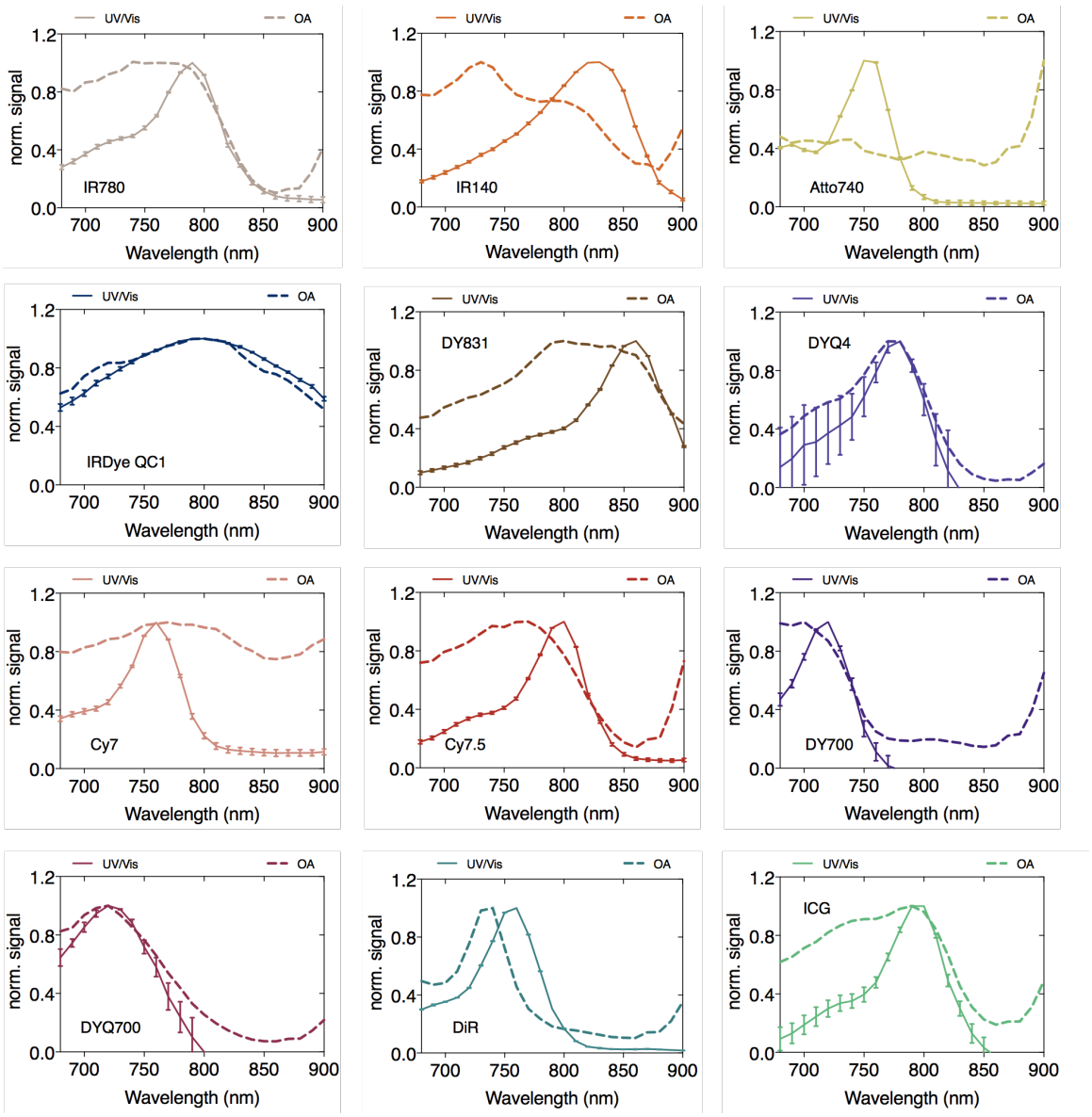

Figure S15: **Absorbance and optoacoustic spectra of near-infrared sonophores, IR780, IR140, Atto740, IRDye QC-1, DY831, DYQ4, Cy7 COOH, Cy7.5 COOH, DY700 COOH, DYQ700 COOH, DiR, ICG.** Normalized UV/Vis absorbance (solid lines) and phantom MSOT measurements (dashed lines) of near-infrared sonophores (10 µM). Measurements were carried out from 690–900 nm based on the imaging capabilities of the MSOT. The data were normalized to its absorbance and optoacoustic maxima of individual sonophores. See Supporting Table 1.

dyes	UV/Vis absorbance (nm)	OA maxima (nm)	ε (M^{-1} cm^{-1})	QY	nanoemulsions	UV/Vis absorbance (nm)	OA maxima (nm)	size (nm)	pdi	ζ- potential	NE particle (nM)	loading conc. (μM)
IR-780	790	770	156,000	0.17	NE-IR780	800	810	145 ± 5.9	0.137 ± 0.014	-6.12 ± 1.33	0.747 ± 0.017	8.55
IR-140	830	730	140,000	0.12	NE-IR140	960	-	133 ± 1.4	0.131 ± 0.041	-1.00 ± 1.91	0.561 ± 0.011	15.09
ATTO740	750	730	91,000	0.10	NE-ATTO740	745	730	119 ± 8.5	0.153 ± 0.043	-2.85 ± 1.85	0.226 ± 0.006	0.79
IRDye QC-1	800	800	98,000	0	NE-IRDye QC1	750	810	149 ± 5.8	0.131 ± 0.013	-4.20 ± 0.76	0.438 ± 0.008	0.56
DY831	860	800	311, 000	0.02	NE-DY831	835	820	137 ± 2.5	0.141 ± 0.023	-7.46 ± 0.10	0.586 ± 0.011	2.70
DYQ4	780	780	60,000	0	NE-DYQ4	760	750	148 ± 6.9	0.132 ± 0.033	-3.01 ± 0.93	0.463 ± 0.027	8.64
Cy7	760	700	206,000	0.30	NE-Cy7	765	760	147 ± 4.0	0.121 ± 0.017	-1.79 ± 1.15	0.277 ± 0.016	7.46
Cy7.5	800	720	262,000	-	NE-Cy7.5	810	810	141 ± 4.4	0.122 ± 0.046	-7.30 ± 1.62	0.608 ± 0.017	4.39
DY700	720	770	84,000	0.047	NE-DY700	710	700	137 ± 1.3	0.097 ± 0.025	-0.24 ± 0.58	0.385 ± 0.027	3.49
DYQ700	720	770	48,000	0	NE-DYQ700	690	700	141 ± 1.7	0.105 ± 0.024	-3.36 ± 1.47	0.709 ± 0.002	17.71
DiR	760	740	210,000	0.25	NE-DiR	750	740	144 ± 4.5	0.105 ± 0.055	-1.79 ± 1.15	0.507 ± 0.027	9.55
ICG	800	790	140,000	0.04	NE-ICG	810	800	137 ± 0.7	0.112 ± 0.028	-2.88 ± 4.09	0.610 ± 0.011	21.20

Table S1: **Summary of the physical and optoacoustic characterizations of near-infrared and nanoemulsion sonophores.** (*left*) The UV/Vis absorbance maxima *vs.* the optoacoustic maxima for free dyes (10 μM) are reported together with the corresponding extinction coefficients (ε) and quantum yields (QY). (*right*) The UV/Vis absorbance *vs.* optoacoustic maxima for the near-infrared nanoemulsions, with their corresponding mean effective diameters (nm), polydispersity indeces (pdi), mean zeta-potentials, nanoparticle concentrations (nM) and loading concentrations of dye (μM).

a

near infrared dye		high	medium	low
IR780	dye	0.123	0.247	0.130
	NE	0.089	0.257	0.607
IR140	dye	0.695	0.610	0.779
	NE	0.177	0.408	0.411
Atto740	dye	0.232	0.222	0.155
	NE	0.898	1.160	2.194
IRDye QC1	dye	1.104	2.493	1.944
	NE	3.976	4.924	5.658
DY831	dye	1.035	3.700	3.781
	NE	0.431	1.194	1.436
DYQ4	dye	0.149	1.214	6.181
	NE	0.184	0.254	0.498
Cy7	dye	0.068	0.060	0.087
	NE	0.115	0.181	0.338
Cy7.5	dye	0.344	0.638	0.528
	NE	0.096	0.336	0.302
DY700	dye	0.252	0.585	0.675
	NE	0.397	0.456	0.402
DYQ700	dye	0.419	0.837	1.352
	NE	0.377	0.493	1.427
DiR	dye	0.377	0.493	1.427
	NE	0.280	0.436	0.842
ICG	dye	0.352	0.524	0.521
	NE	0.061	0.276	0.360

b

Figure S16: **OA signal change due to molecular stacking in the NEs.** (a) Tabulated OA signal in arbitrary units for NIR dyes in solution and in NE formulation normalized by the concentration of molecules in micromolar (μM). (b) The relative log ratio change of signal for each dye between intensity in NE vs. intensity in solution. The signal emanated on a per molecule basis depends on the concentration of dye within the NE as well as the concentration of the NE colloid. For example, the OA signal of ICG decreases when in NE vs. when in solution. IRDye QC1 demonstrates the highest signal enhancement when encapsulated in low concentration NEs.

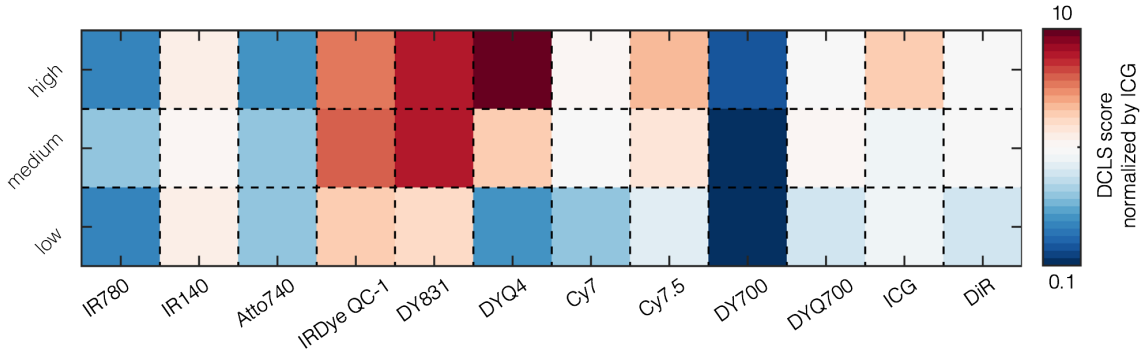

Figure S17**: MSOT imaging of the small molecule sonophores in soft-tissue mimicking phantoms.** The twelve small molecule sonophores were imaged using the MSOT. At higher concentrations (high and medium) DYQ4, DY831 and IRDye QC1 are the best performing small molecule sonophores respectively. At lower concentrations (low), IRDye QC1 appears to be the best performing sonophore.

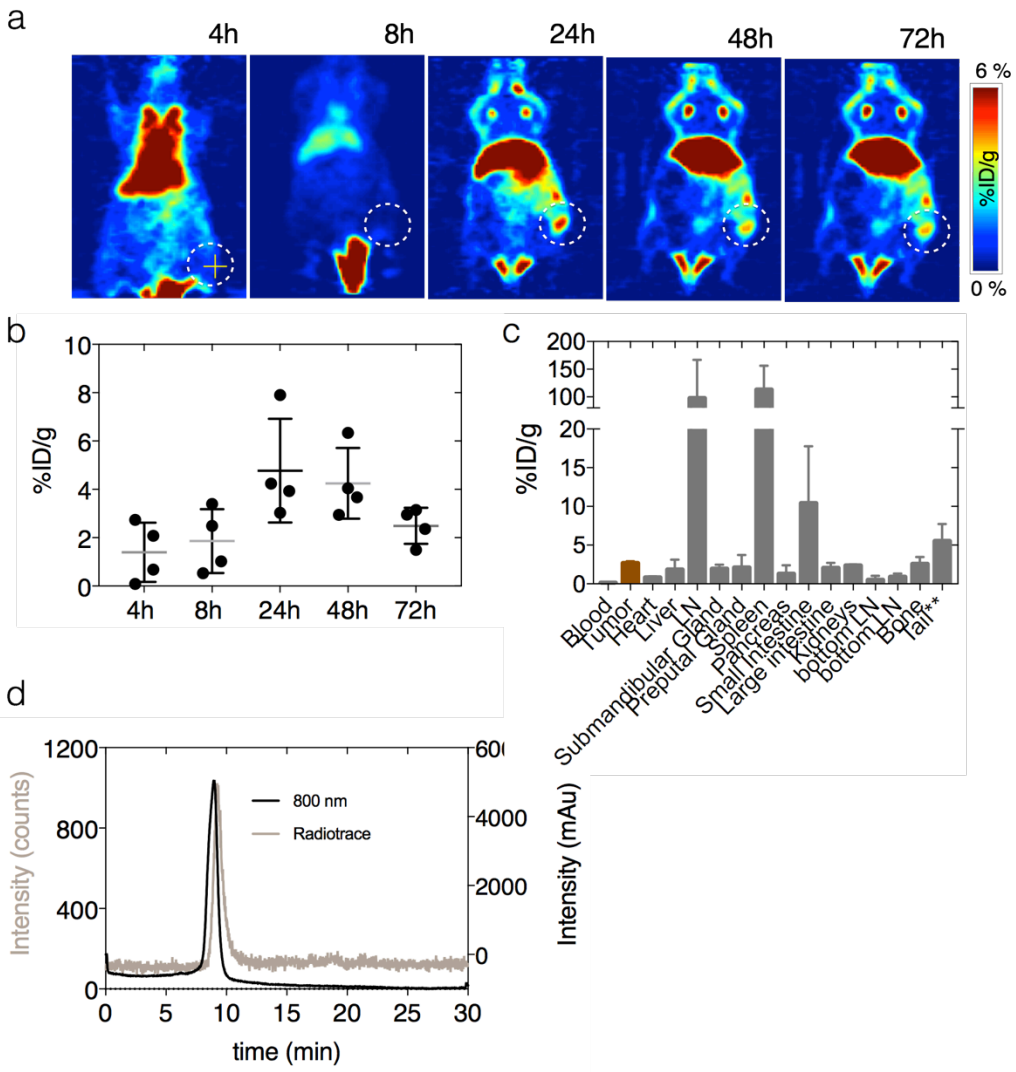

Figure S18: ***In vivo* kinetics and biodistribution validation of near-infrared nanoemulsion using positron emission tomography (PET).** (A) Representative PET *in vivo* images of radiolabelled ^{89}Zr-NE-IR780 using murine breast cancer model 4T1. Mice (n = 4) were injected (i.v.) with 195-205 µCi of ^{89}Zr-NE-IR780 and imaged *via* PET at 4h, 8h, 24h, 48h and 72h post injection. Images showed optimal tumor uptake at 24h. There were high accumulation of NE-IR780 in lymph nodes (LN) and spleen, typical of nanoemulsions with similar size. (B) Quantification of PET images from the tumor region of interests (ROI) (C) The tissue biodistribution data (%ID/g) of ^{89}Zr-NE-IR780 at 72h. (D) Size-exclusion chromatogram showing radioactive trace of ^{89}Zr-NE-IR780 and the purity of sample before i.v. injection.

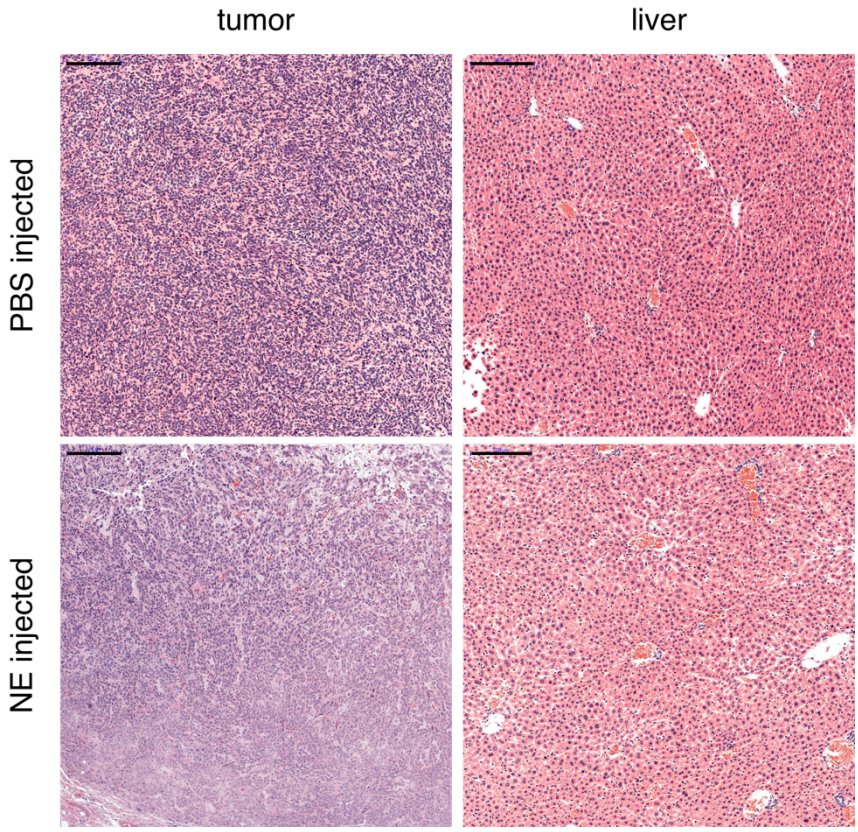

Figure S19: **Toxicity studies of nanoemulsion in murine breast cancer model 4T1.** Histology of tumor (*left)* and liver (*right*) tissue section, stained with hematoxylin and resin (H&E) showed normal morphology indicative of healthy cells in both control (PBS injected) and nanoemulsion NE-IRDye QC1 treated group (NE injected) at 24h post i.v. injection. Liver treated with NE-IRDye QC1 showed normal hepatocytes with clear portal vien, bile duct and hepatic arteriole (200 μM scale bar) 100% survival was observed in mice injected with nanoemulsion NE-IRDye QC1.

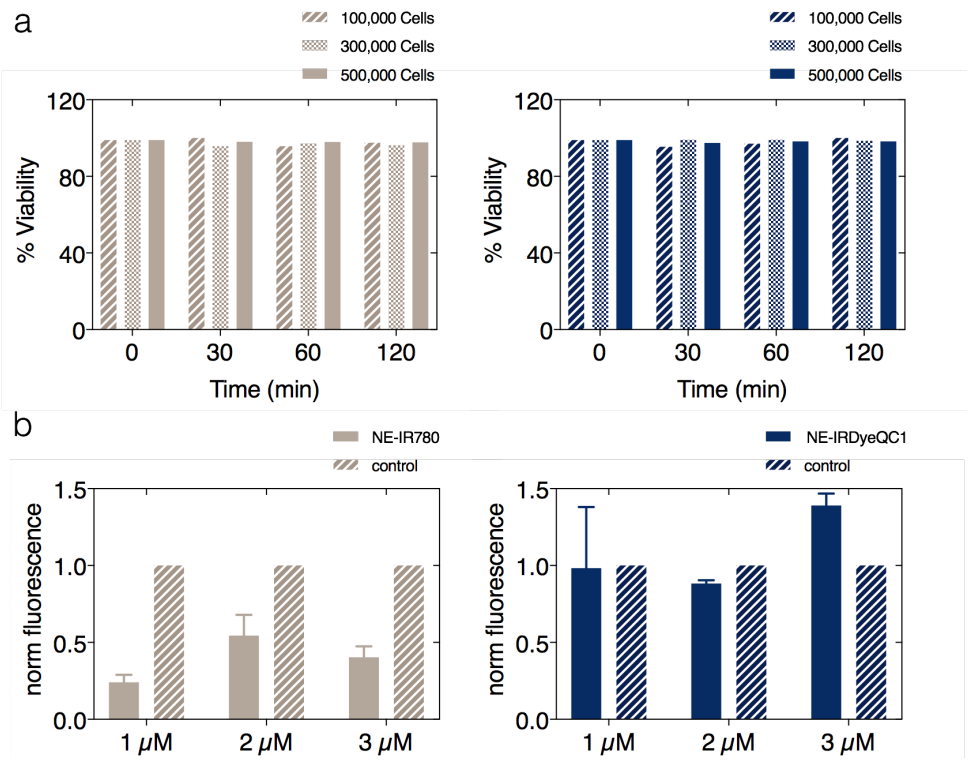

Figure S20: **Cell viability assessment of NE-IR780 and NE-IRDye QC1 using Trypan Blue and testing survival using alamarBlue® Assay.** (a) Varying number of 4T1 cells (100, 000, 300,000 and 500,000) were incubated with 1 μM of either NE-IR780 (*left*) or NE-IRDyeQC1 (*right*) at various timepoints indicated on the graphs above. Trypan Blue viability test was carried out by diluting cell sample in Trypan Blue dye in DMEM in 1:1 dilution cell suspension using 0.4% Trypan Blue solution showed >98% cell survival after nanoemulsion treatment. (b) Survival assay using varying concentrations (1 μM, 2 μM and 3 μM) alamarBlue® treatment for 4 h, data shows better cell survival with NE-IRDyeQC1.

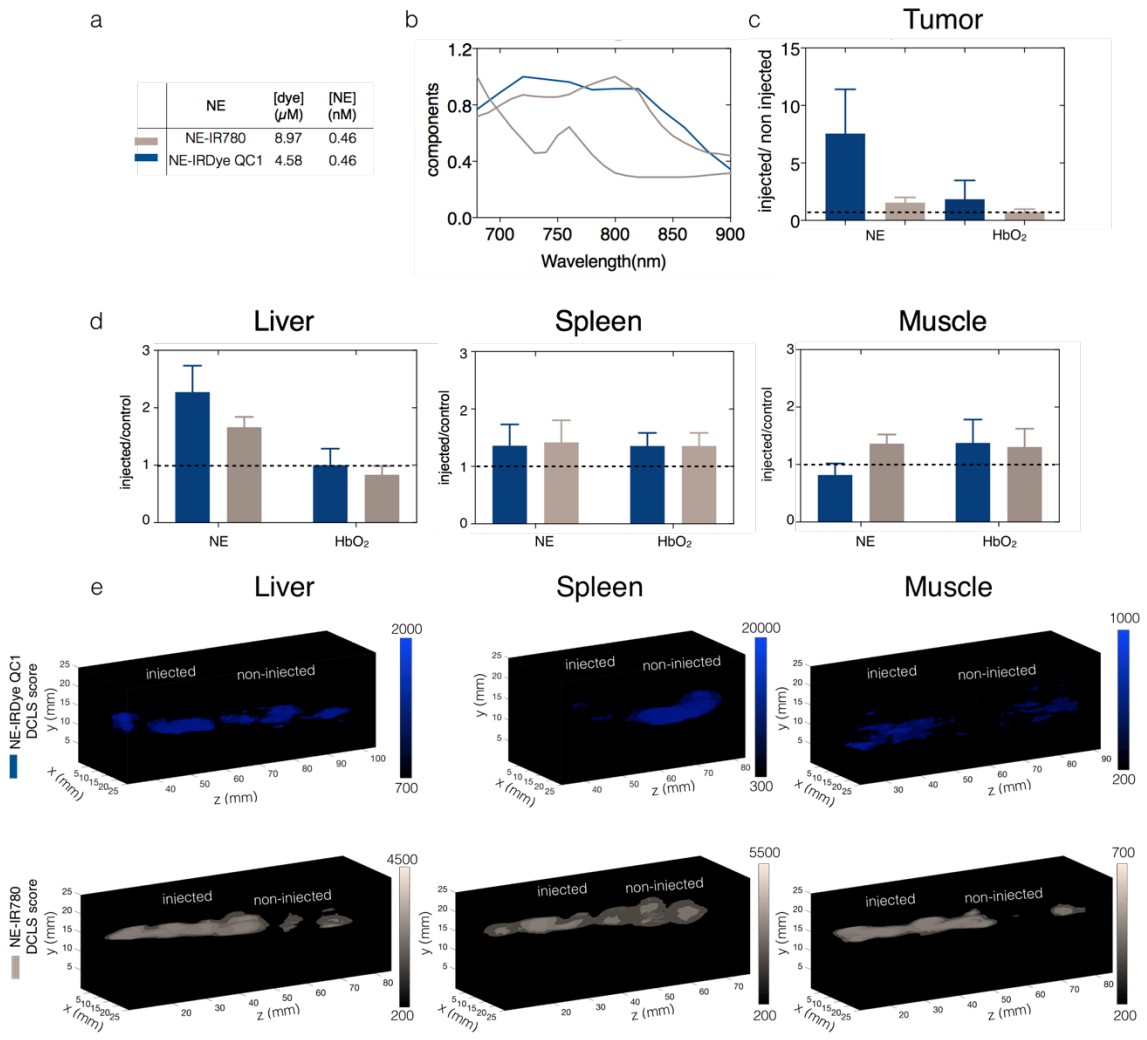

Figure S21: ***Ex vivo*** **optoacoustic imaging of NE-IRDye QC1 and NE-IR780 in a 4T1 tumor model, 24h after intravenous injections using the multi-spectral optoacoustic tomography (MSOT).** (a) The dye and nanoemulsion concentrations of NE-IRDye QC1 and NE-IR780 injected. (b) Normalized references of blood, NE-IRDye QC1 and NE-IR780 used for the spectral unmixing. (c) The injected to non-injected group ratio comparison between NE-IRDye QC1, and NE-IR780 for ex-vivo tumor MSOT imaging. (d) The injected to non-injected group ratio comparisons between NE-IRDye QC1 and NE-IR780 for ex-vivo liver, spleen and muscle MSOT imaging. (e) *Ex vivo* optoacoustic image reconstruction of NE-IRDye QC1 for non-injected and injected group of liver, spleen and muscle (*top*) and the corresponding image reconstructions for NE-IR780 (*bottom*).

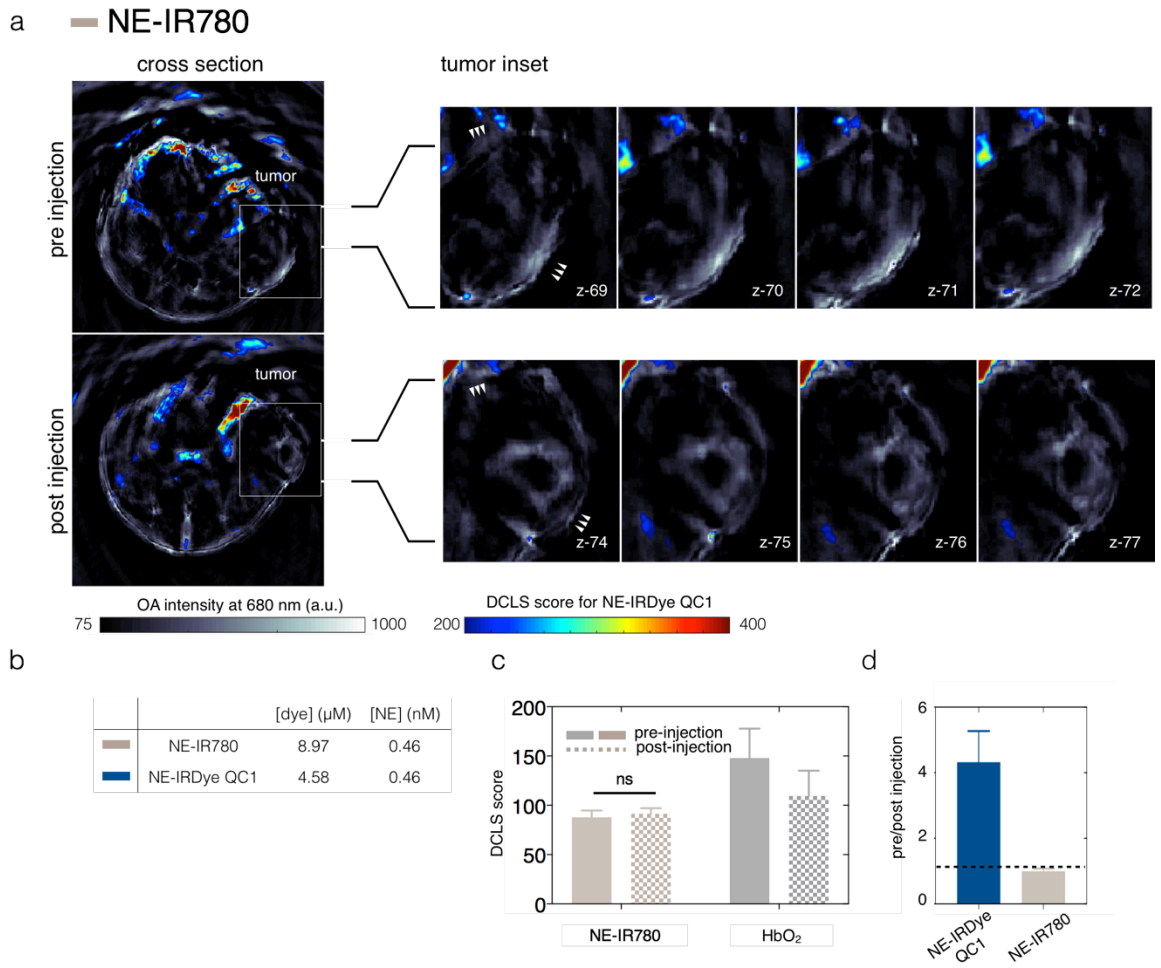

Figure S22: ***In vivo* accumulation of nanoemulsion (NE) NE-780 in a 4T1 tumor model 24 h after intravenous injection using multi-spectral optoacoustic tomography (MSOT)**. (a) Transverse MSOT image of a 4T1 tumor-bearing mouse (n = 4) are shown before (top) and after (bottom) using 810 nm illumination wavelength (bone color scale) as background and overlaid with NE-IR780 signature scoring using a direct least-squares (DCLS) model based technique (jet color scale). Several axial positions were imaged and the tumor insets (*right*) are from the three different positions showing the distribution of NE-IR780 throughout the tumor. (b) The dye and nanoemulsion concentrations of NE-780 and NE-IRDye QC1 for injected. (c) Corresponding optoacoustic signal quantification of *in-vivo* MSOT images. (d) Pre-injection to post-injection tumor ratio of NE-IRDye QC1 and NE-IR780.